International Seminar on Student Research in Education, Science, and Technology
ISSN 3047-1532 | Volume 2 April 2025, pp. 151-161

https://www.issrestec.id/
http://journal.ummat.ac.id/index.php/issrestec
Universitas Muhammadiyah Mataram, Indonesia

Experimental and Numerical Study of Non-Pneumatic Tires with Honeycomb Structure on Varying Road Inclination Angles

Zahran Ra'if Agustiara[1], Rachmat Sriwijaya[1]
[1]Departemen Teknik Mesin dan Industri, Fakultas Teknik, Universitas Gadjah Mada, Indonesia
zahranraif@mail.ugm.ac.id, sriwijaya@gadjahmada.edu

Abstract: The increasing demand for vehicle mobility necessitates advancements in tire technology, with non-pneumatic tires (NPT) emerging as a promising alternative. NPTs address key limitations of conventional pneumatic tires, such as puncture risks and air pressure dependency. The honeycomb structure in NPTs is engineered to enhance load-bearing capacity and shock absorption, yet its performance under varying road inclination angles remains underexplored. This study integrates both experimental and numerical methodologies using the Finite Element Method (FEM). Three distinct NPT models with varying honeycomb cell angles were tested on inclined road surfaces (0°, 10°, and 20°). Experimental trials were conducted with a Universal Tensile Machine (UTM) to evaluate vertical reaction forces, while numerical simulations in ANSYS validated experimental outcomes under dynamic conditions. Key parameters such as von Mises stress distribution and stiffness were analyzed. Findings indicate that NPT models with smaller honeycomb cell angles exhibit higher vertical reaction forces, suggesting superior load-bearing capabilities on inclined surfaces. This research provides critical insights for optimizing NPT designs, particularly in applications where stability and durability are essential.

Keywords: Non-Pneumatic Tires, Honeycomb Structure, Finite Element Method, Road Inclination, Vertical Reaction Forces.

Article History:
Received: 01-04-2025
Online : 24-04-2025

A. INTRODUCTION

The rapid advancement of vehicle mobility has led to increasing demands for innovative tire technologies that offer improved performance, durability, and safety. Non-pneumatic tires (NPTs) have emerged as a potential alternative to conventional pneumatic tires, addressing issues such as air pressure dependency, puncture risks, and maintenance requirements (Jin et al., 2018). Instead of relying on compressed air, NPTs utilize a structured support mechanism, such as honeycomb configurations, to bear loads and absorb shocks (Ju et al., 2012). This unique structural approach enhances load distribution, structural integrity, and impact resistance, making NPTs a promising solution for various applications, including off-road vehicles, military vehicles, and autonomous transportation systems. However, despite the potential advantages of NPTs, their mechanical behavior under varying road inclination angles remains insufficiently explored. The performance of an NPT is significantly influenced by the geometric properties of the honeycomb structure, which determines its stiffness, energy absorption, and deformation characteristics (Li et al., 2023). Previous research has demonstrated that honeycomb structures with different cell angles and dimensions exhibit variations in stress distribution, load-bearing capacity, and energy

absorption (Ju et al., 2012). For instance, Li et al. (2023) found that hexagonal honeycomb structures provide superior energy absorption due to their even load distribution and high structural stability compared to other geometric configurations.

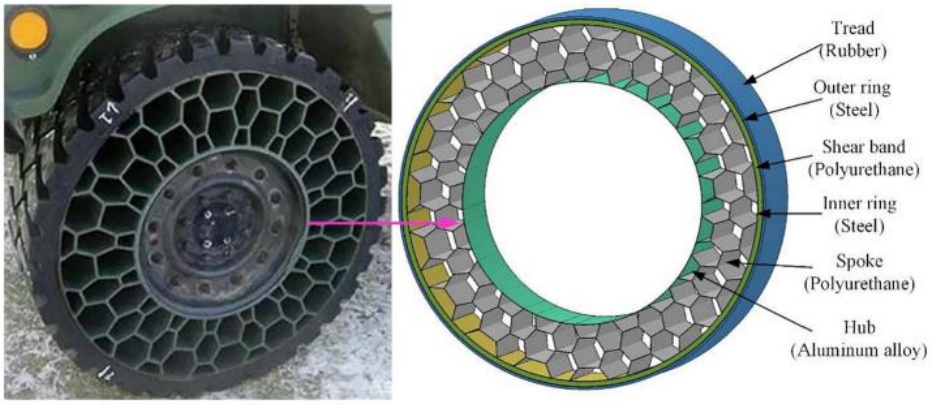

Figure 1. NPT honeycomb and its construction (Jin et al., 2018).

Several studies have investigated the static and dynamic mechanical properties of NPTs. Sriwijaya and Hamzah (2019) conducted simulations on NPTs with honeycomb structures under static loading conditions and found that higher inclination angles result in increased stress concentration and deformation patterns. Similarly, Jin et al. (2018) analyzed the influence of external loading on NPTs and observed that dynamic loading conditions lead to higher Von Mises stress values compared to static conditions. Furthermore, research by Wang et al. (2024) emphasized the importance of vertical stiffness in NPTs, showing that different honeycomb configurations significantly affect force-displacement responses and fatigue resistance. However, a comprehensive study integrating both experimental and numerical methods under varying road inclinations has not been extensively conducted. To address this research gap, this study employs a combined experimental and numerical approach using the Finite Element Method (FEM) to analyze the mechanical behavior of NPTs under different road inclination angles.

B. METHOD

This study integrates both experimental and numerical methodologies to comprehensively assess the mechanical behavior of three NPT models with varying honeycomb cell angles are tested under inclination angles of 0°, 10°, and 20° to evaluate their vertical reaction forces, stress distribution, and stiffness characteristics. The experimental analysis is conducted using a Universal Tensile Machine (UTM), while numerical simulations are performed using ANSYS to validate the results.

1. Geometry Modelling of NPTs

The NPT models are designed with a honeycomb spoke structure, replacing the conventional air-filled cavity. Three distinct honeycomb cell angles are analyzed to evaluate their effects on mechanical performance. The three NPT models maintain a constant outer diameter (ϕD_s = 104 mm), inner diameter (ϕd_s= 55.61 mm), and spoke width (w = 40.98 mm)

while varying the honeycomb cell angles: Model A (θ = 13.51°), Model B (θ = 22.67°), and Model C (θ = 30.75°) as shown in Table 1.

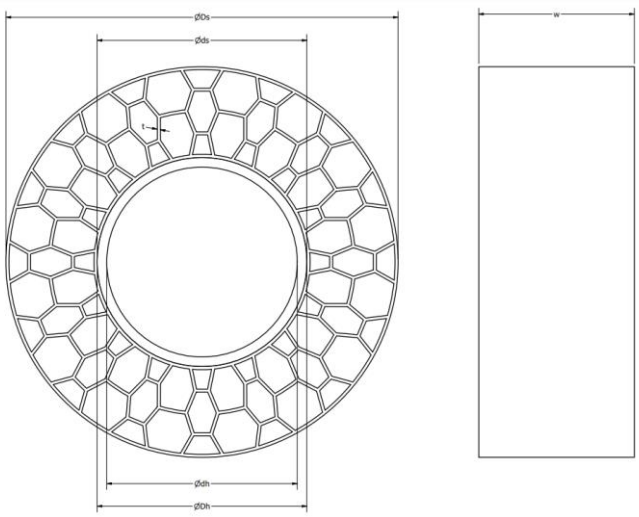

Figure 2. Parameter spoke model

Table 1. Geometrical dimensions of the spoke model

Parameter	Size (mm)
Spoke outer diameter (ϕD_s)	104
Spoke inner diameter (ϕd_s)	55.61
Hub outer diameter (ϕD_h)	55.60
Hub inner diameter (ϕd_s)	50.55
Spoke thickness (t)	0.8
Spoke width (w)	40.988

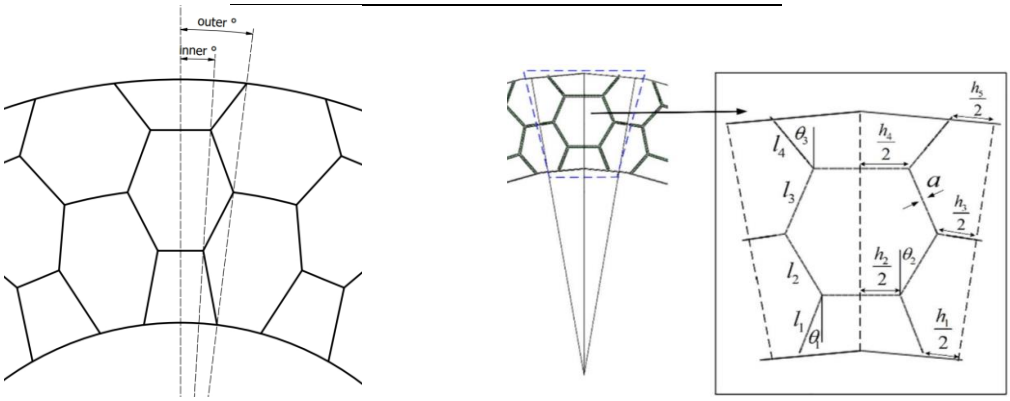

Figure 3. Variation of cell angle at honeycomb structure (Jin et al., 2018)

Table 2. Geometrical parameters of honeycomb cell configurations for NPT types

Type	Outer (°)	Inner (°)	l_{avg} (mm)	$h/2_{avg}$ (mm)	θ_{avg} (°)
NPT A	4	6	6.02	3.32	13.51
NPT B	3,5	7	6.35	2.76	22.67
NPT C	2,5	7,5	6.83	2.27	30.75

2. Material Selection and Property Characterization

The NPT models are fabricated using thermoplastic polyurethane (TPU) for the spoke structure and acrylonitrile butadiene styrene (ABS) for the hub. The material properties are determined through tensile testing following ASTM D638 standards. The experimental tensile tests are conducted using a universal tensile machine (UTM) to determine Young's modulus, tensile strength, and Poisson's ratio. TPU, selected for its flexibility and impact resistance, has an experimentally measured Young's modulus of 26–39 MPa (León-Calero et al., 2021), while ABS, chosen for its structural rigidity, has a modulus of 2300–2600 MPa (Oosthuizhen et al., 2013; Chen et al., 2017). The numerical simulations further validate these material properties to ensure consistency between experimental and computational models.

Table 3. Summary of material properties used in NPT components (León-Calero et al., 2021; Oosthuizhen et al., 2013; Chen et al., 2017)

Material Properties	Thermoplastic Polyurethane	Acrylonitrile Butadiene Styrene
Density (kg/m^3)	1200	1000-1200
Young Modulus (MPa)	26-39	2300-2600
Poisson's Ratio (-)	0.4	0.35-0.38

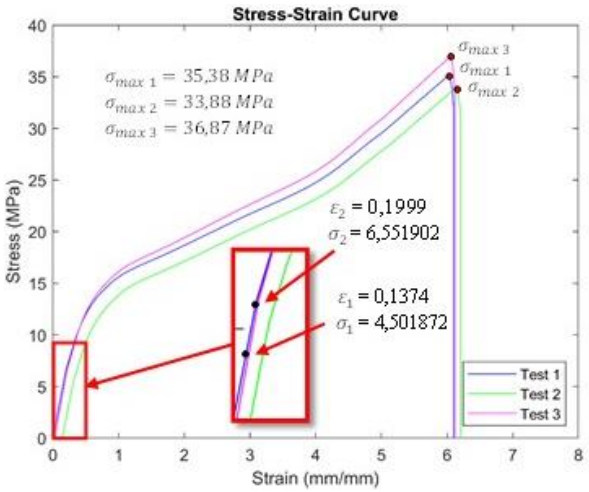

Figure 4. Stress-strain curve tensile test for thermoplastic polyurethane

The stress-strain curve obtained from the tensile test is shown in Figure 4. This graph is used to determine Young's Modulus and yield strength values using Equations 1 and 2. The obtained values were then validated by comparing them with the material property values from the manufacturer's datasheet and previous research, as presented in Table 3. Based on the range of Young's Modulus and yield strength values obtained from the datasheet references and previous studies, it can be concluded that the Young's Modulus and yield strength values obtained from the tensile tests are still in agreement with the estimated values for both Young's Modulus and yield strength ($E = 32.77\ MPa;\ S_y = 32.38\ MPa$). Therefore, the values obtained from the tensile test are considered to accurately represent the material properties of TPU 95A, which will be used in the simulations.

$$E = \frac{\sigma_2 - \sigma_1}{\varepsilon_2 - \varepsilon_1} \quad (1)$$

$$S_y = \frac{\sigma_{max1} + \sigma_{max2} + \sigma_{max3}}{3} \quad (2)$$

3. Setup and Testing

The experimental study is conducted using a universal tensile machine (UTM) coupled with a mini-conveyor system that simulates rolling conditions at different inclination angles (0°, 10°, and 20°). The UTM is used to apply vertical loads and measure reaction forces, deformation, and stress distribution. The experimental apparatus consists of three primary components: (1) a universal tensile machine and (2) a mini conveyor system that allows for adjustable inclination angles. The mini conveyor system operates at 0.09 m/s speed, with rollers of 50 mm diameter. During the experiment, the NPT prototype is mounted onto the UTM's crosshead, with the conveyor belt positioned underneath to simulate rolling conditions. A constant displacement rate of 1 mm is applied to evaluate the tire's mechanical response at each inclination angle. The vertical reaction force is measured using load cells. The force-time data are processed using EMTT (Electrical Mechanical Tensile Test) software, which provides real-time data visualization and ensures experimental accuracy.

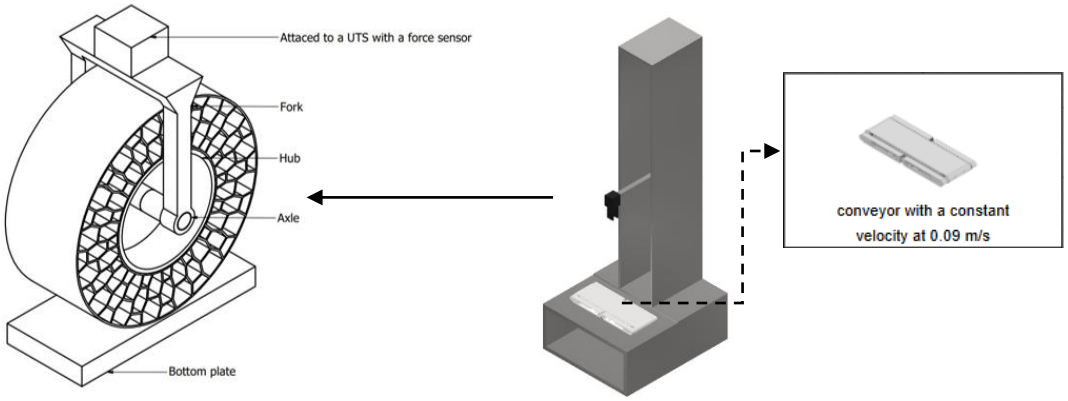

Figure 5. Experiment Setup

In this study, the Finite Element Analysis (FEA) is performed using the Explicit Dynamics Module in ANSYS 2020 R2 to simulate the dynamic response of non-pneumatic tires (NPTs) under inclined road conditions. In explicit dynamics, the system is solved step by step over time using time integration, where the displacement and velocity are updated as in Equations 3 and 4. The time step Δt, which determines how much the system updates at each step, is critical for stability. In explicit methods, this time step is determined by the Courant-Friedrichs-Lewy (CFL) stability criterion, which is given by equation 5, where L_{min} is the smallest element length in the mesh, and c is the wave speed within the material, with E being the Young's modulus and ρ the density of the material. This formula ensures that the time step is small enough to maintain numerical stability, particularly when dealing with high-frequency vibrations or shock loads. These governing equations and the CFL time step formula play a crucial role in ensuring the accuracy and stability of the numerical simulation,

providing detailed insights into the dynamic behavior of NPTs under various loading conditions (ANSYS, 2020).

$$\dot{u}_{i+1/2} = \dot{u}_{i-1/2} + \Delta t \ddot{u}_i \quad (3)$$

$$\dot{u}_{i+1/2} = u_i + \Delta t \dot{u}_{i+1/2} \quad (4)$$

$$\Delta t = \frac{L_{min}}{c}, c = \sqrt{\frac{E}{\rho}} \quad (5)$$

C. RESULTS AND DISCUSSION

1. Manufacturing of the NPT Prototype

The NPT prototypes were fabricated using Fused Deposition Modeling (FDM) 3D printing technology (Haid et al., 2022), specifically with eSun TPU 95A filament for the honeycomb spokes and ABS material for the hub structure. The image above shows the final prototype with its key components labeled, including the spoke, hub, fork, and axle. The spoke is the main load-bearing component of the tire, while the hub connects the tire to the vehicle's axle. The fork and axle serve as the central structural elements for connecting the NPT to the vehicle, providing rotational support.

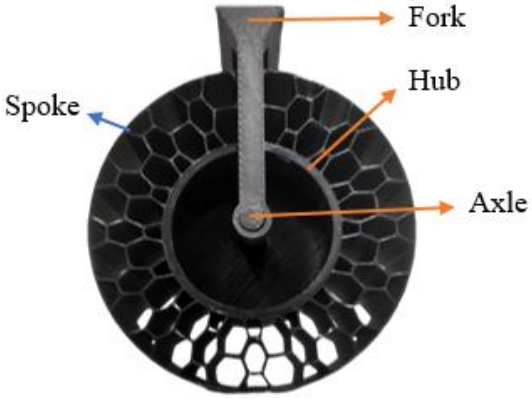

Figure 6. Prototype of NPT

The 3D printing parameters used during fabrication are detailed in Table 4, which includes important settings. These settings were chosen to optimize the quality and consistency of the printed tire, ensuring that the honeycomb structure maintains its mechanical properties. The infill of 100% ensures the tire's core is solid, providing maximum strength, while the layer height of 0.16 mm ensures a fine resolution for printing the intricate honeycomb pattern. The nozzle temperature of 210°C and bed temperature of 50°C are optimal for the eSun TPU 95A filament, ensuring good adhesion to the printing surface and reducing the risk of warping during the print. Incorporating these 3D printing parameters into the design process ensures that the physical properties of the prototypes align with the specifications used in the finite element analysis (FEM) in ANSYS.

Table 4. Printing parameter for the prototype of spoke NPT

Parameters	Value	Units
Infill	100	%
Nozzle temperature	210	$°C$
Layer height	0.16	mm
Bed temperature	50	$°C$
Printing speed	15	mm/s

2. Von Mises Stress and Vertical Reaction Force

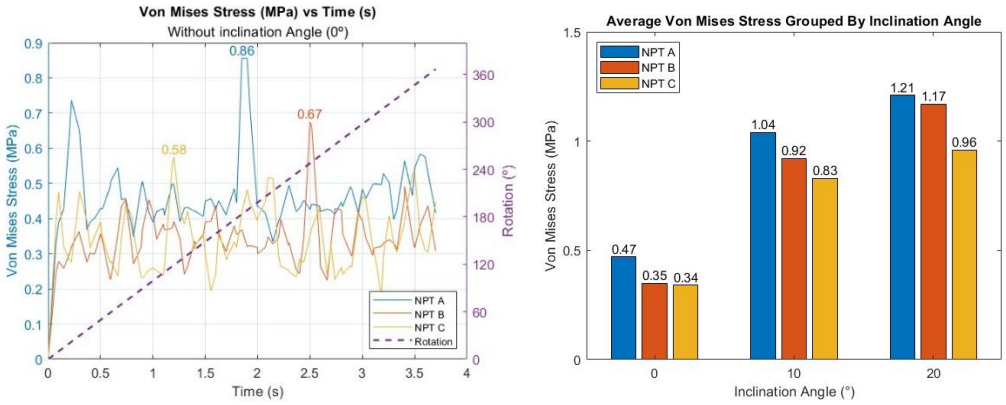

Figure 7. Von Mises Stress under dynamic load (left) and average Von Mises stress for each variation (right)

The first plot in Figure 7 shows the Von Mises stress evolution over time for the three NPT models under a flat surface. The stress response of the models is presented for a period of 3.7 seconds. The data indicates that NPT A experiences the highest peak stress of 0.86 MPa, as compared to NPT B and NPT C, which exhibit lower peak values. This suggests that NPT A, with the smallest honeycomb cell angle, concentrates stress more locally, particularly during dynamic loading conditions. In contrast, NPT C, with the largest honeycomb cell angle, distributes the stress more evenly, leading to a lower peak stress of 0.67 MPa. The plot also shows the rotation (in degrees), which is tracked simultaneously during the simulation. The correlation between stress and rotational behavior is highlighted, with higher stress values often corresponding to larger rotation angles, indicating that the structural rigidity and deformation behavior influence each other during loading. The second figure presents the average Von Mises stress for the three NPT models across three different road inclination angles (0°, 10°, and 20°). The bars represent the average stress for each model at the specified angles. At 0° inclination, the average Von Mises stress for NPT A is 0.47 MPa, significantly higher than NPT B (0.35 MPa) and NPT C (0.34 MPa), indicating that NPT A provides greater resistance to deformation under flat conditions. As the inclination angle increases, the Von Mises stress increases for all models. This trend, observed at 10° and 20° inclinations, follows a similar pattern, with NPT A continuing to show the highest stress values, while NPT C displays the lowest, and NPT B falls in between, demonstrating a balance between the other two models.

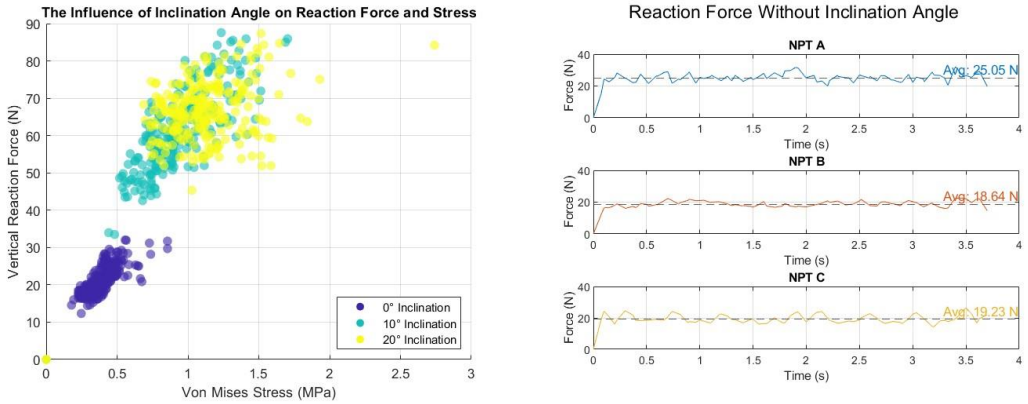

Figure 8. The Influence of Road Inclination Angle on Vertical Reaction Force and Von Mises Stress (left) and Vertical Reaction Force Without Inclination Angle for the Three NPT Models (right)

The scatter plot in Figure 8 shows the relationship between Von Mises stress and vertical reaction force for the three NPT models under varying road inclination angles. Each data point corresponds to a specific time step during the simulation, providing insight into how the reaction force and stress change dynamically during loading. From the plot, it is evident that as the inclination angle increases, both stress and reaction force generally increase, with the 20° inclination showing the highest stress and reaction force values across all NPT models. NPT A consistently exhibits higher reaction forces and stress levels compared to NPT B and NPT C, which suggests that smaller honeycomb cell angles provide greater rigidity and load resistance. However, the data also reveals significant variability in reaction force and stress for each inclination angle, highlighting the complex interaction between honeycomb geometry and road conditions. The second figure shows the reaction force over time for each NPT model under 0° inclination (flat surface). The average reaction force for each model is also indicated at the top of each plot. For NPT A, the reaction force fluctuates around an average of 25.05 N, showing relatively consistent behavior with higher spikes compared to the other models. NPT B shows a slightly lower average reaction force of 18.64 N, reflecting its more flexible honeycomb structure, which leads to lower load resistance. NPT C exhibits the lowest average reaction force of 18.23 N, suggesting it has the least stiffness and the greatest deformation potential under flat conditions. These trends further confirm the influence of honeycomb cell geometry on the dynamic load-bearing capacity of the tire.

3. Stiffness of NPTs

Figure 9 presents the force-displacement relationship for different NPT configurations. The graph compares the performance of three NPT models in terms of their stiffness under compression. Each model's behavior is depicted by a solid line, with the corresponding linear fit shown by the dotted lines. The graph clearly shows that NPT A exhibits the highest stiffness, with a force-displacement slope of 18.29 N/mm. This is due to its smaller honeycomb cell angle, which makes the structure stiffer and more resistant to deformation under load. NPT B follows with a stiffness of 12.23 N/mm, reflecting its moderate

honeycomb geometry that strikes a balance between rigidity and flexibility. NPT C, with the largest honeycomb cell angle, shows the lowest stiffness of 13.82 N/mm, indicating greater flexibility and deformation under applied loads. The linear fit for each model, represented by the dotted lines, confirms the linear nature of the force-displacement relationship, with NPT A consistently showing the highest force at each displacement value. This highlights the impact of honeycomb geometry on the structural performance of non-pneumatic tires, where smaller angles provide greater stiffness, and larger angles lead to more flexibility.

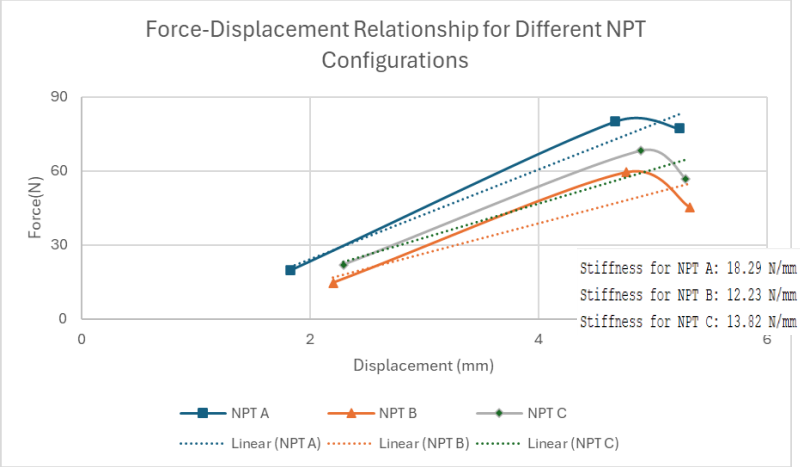

Figure 9. Force-displacement relationship for different NPT configurations

4. Numerical Results and Experimental Validation

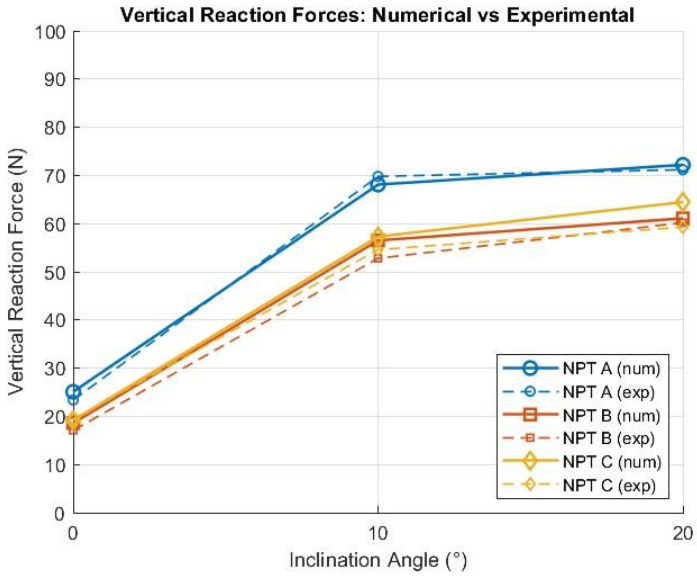

Figure 10. Comparison of Vertical Reaction Force Values: Numerical and Experimental Methods

Figure 10 shows the comparison of vertical reaction forces between numerical simulations and experimental results. The solid lines represent experimental data, while the dashed lines indicate numerical results. As the inclination angle increases, the vertical reaction force rises for all models. NPT A consistently exhibits the highest vertical reaction force, followed by NPT B and NPT C, which show the lowest reaction force. The plot also shows a strong agreement between numerical and experimental results, validating the accuracy of the ANSYS simulations in predicting the tire's response under dynamic conditions. The small discrepancies between the two datasets are likely due to experimental measurement variations and simulation assumptions. This figure highlights the reliability of numerical simulations in predicting the vertical reaction force of NPTs under inclined loading conditions.

D. CONCLUSIONS AND SUGGESTIONS

This research demonstrates that NPTs with smaller honeycomb cell angles exhibit higher structural stiffness, resulting in increased vertical reaction forces and Von Mises stresses while maintaining minimal deformation under loading. Conversely, NPTs with larger cell angles show lower stress concentrations but undergo greater deformation due to their increased flexibility. An increase in road inclination angle leads to a corresponding rise in vertical reaction force and stress distribution across all NPT configurations. These effects are more pronounced in stiffer designs. The numerical simulation results exhibit strong agreement with experimental data in terms of observed trends, validating the predictive capability of the finite element model despite certain limitations related to surface interaction and environmental conditions. From a design standpoint, no single honeycomb configuration proves universally optimal. NPT A is well-suited for high-load applications due to its rigidity, NPT C offers enhanced comfort and adaptability on uneven terrains, while NPT B provides a balanced compromise between stiffness and flexibility, making it the most versatile option across varying operational conditions.

REFERENCES

ANSYS, 2020. ANSYS Explicit Dynamics Analysis Guide (release 2020R1). ANSYS, Inc.

Chen, D. C., Lai, B. Y., & Gao, F. Y. (2017). Simulation analysis of turbine blade in 3D printing aquarium. In *MATEC Web of Conferences* (Vol. 123, p. 00008). EDP Sciences.

Haid, D. M., Duncan, O., Hart, J., & Foster, L. (2022). Characterisation of thermoplastic polyurethane (TPU) for additive manufacturing.

Jin, X., Hou, C., Fan, X., Sun, Y., Lv, J., & Lu, C. (2018). Investigation on the static and dynamic behaviors of non-pneumatic tires with honeycomb spokes. *Composite Structures*, *187*, 27-35.

Ju, J., Kim, D.-M., & Kim, K.-W. (2012). Flexible cellular solid *spoke*s of a non-pneumatic tire. *Composites Science and Technology*, *72*(12), 2285-2295.

León-Calero, M., Reyburn Valés, S.C., Marcos-Fernández, Á., & Rodríguez-Hernandez, J. (2021). 3D Printing of Thermoplastic Elastomers: Role of the Chemical Composition and Printing Parameters in the Production of Parts with Controlled Energy Absorption and Damping Capacity. Polymers, 13(20), 3551., 13(3), 87-99.

Li, J., Zhong, W., Li, J., Liu, Y., & Zhang, Z. (2023). Influence of Cell Pore Configuration on Dynamic Mechanical Properties of Honeycomb Structures. In *Journal of Physics: Conference Series* (Vol. 2660, No. 1, p. 012006). IOP Publishing.

Oosthuizen, G. A., Hagedorn-Hansen, D., & Gerhold, T. (2013). Evaluation of rapid product development technologies for production of prosthesis in developing communities.

Sriwijaya, R, A, & Hamzah, R, (2019), Simulation study of non-pneumatic tires on varying road inclinations using ABAQUS, Proceedings of the 14th International Conference on Mechanical Engineering, 63-70.

Wang, S., He, P., Geng, Q., Huang, H., Sang, L., & Yao, Z. (2024). Investigation of Additive-Manufactured Carbon Fiber-Reinforced Polyethylene Terephthalate Honeycomb for Application as Non-Pneumatic Tire Support Structure. *Polymers, 16 (1091)*.